ACS APPLIED MATERIALS & INTERFACES

www.acsami.org

Research Article

Investigation of Ethylene and Propylene Production from CO_2 Reduction over Copper Nanocubes in an MEA-Type Electrolyzer

Gastón O. Larrazábal, Valery Okatenko, Ib Chorkendorff, Raffaella Buonsanti, and Brian Seger*

Cite This: *ACS Appl. Mater. Interfaces* 2022, 14, 7779–7787

Read Online

ACCESS | Metrics & More | Article Recommendations | Supporting Information

ABSTRACT: Previous work carried out in fully liquid environments and at low current densities has demonstrated that highly uniform faceted copper nanocrystals display different selectivity profiles in CO_2 reduction compared to polycrystalline copper. As part of ongoing upscaling efforts, it is a matter of interest to investigate whether the high selectivity toward ethylene of copper nanocubes, which show a preferential (100) orientation, is maintained in gas-fed electrolyzers, thus enabling the energy-efficient production of this valuable commodity chemical at industrially relevant current densities. In this work, we assessed the electrochemical CO_2 reduction reaction performance of highly uniform copper nanocubes loaded onto gas diffusion electrodes (GDEs) in a zero-gap device. The copper nanocube-loaded GDEs maintained high Faradaic efficiencies toward ethylene at elevated total current densities, resulting in higher overall partial current densities toward this product compared to benchmark electrodes. Interestingly, CO_2 reduction to propylene, albeit with low partial current densities, was also observed. However, double-layer capacitance measurements revealed that the performance observed at high current densities is significantly influenced by electrode flooding. The findings of this study can inform future efforts geared toward optimizing the electrodes with this promising class of catalysts.

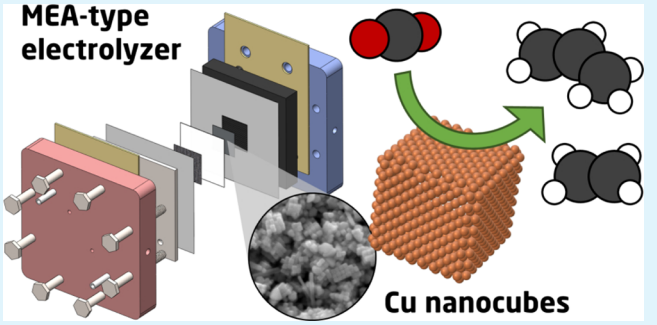

KEYWORDS: *electrocatalysis, CO_2 reduction, copper, nanocrystals, membrane electrode assembly, electrolyzer*

1. INTRODUCTION

The combination of the electrochemical CO_2 reduction reaction (eCO_2RR) with carbon-neutral energy sources offers enticing perspectives for using CO_2 as a sustainable feedstock for the production of fuels and chemicals.[1−3] Research efforts have led to a substantial expansion of the fundamental understanding of CO_2 electroreduction, particularly over copper catalysts, which among transition metals show the unique ability to reduce CO_2 and CO to high-value multicarbon products in substantial amounts.[4−6] It is now well-established that a plethora of factors—including the applied potential, the nature of the electrolyte, local mass transfer characteristics, and, most importantly, the composition and morphology of the catalyst itself—influence the product distribution of the eCO_2RR.[7] In particular, single-crystal studies[8−10] and theoretical works[11] have shed light on the sensitivity of CO_2 and CO electroreduction to the surface morphology of the catalyst, demonstrating that Cu(111) surfaces tend to favor the production of methane, while Cu(100) facets display better selectivity toward high-value multicarbon products, such as ethanol and ethylene. Ethylene is a particularly attractive eCO_2RR product, as it is a major platform chemical with a high market price for which direct production routes not based on fossil feedstocks are lacking.[12] Consequently, there is great interest in exploiting the ethylene selectivity of Cu(100) facets in the eCO_2RR using nanostructured catalysts that mimic the behavior of single-crystal surfaces.

Previous studies have demonstrated that copper nanocubes—which display an abundance of (100)-terminated surfaces—achieve high Faradaic efficiencies for ethylene and low methane production under eCO_2RR conditions.[13,14] This behavior is size-dependent, with 44 nm nanocubes having shown the highest C2 selectivity compared to smaller and bigger particles,[14] which has been ascribed to the existence of a dual-facet mechanism over (100) terraces and (110) edges.[15] However, these encouraging findings from copper nanocubes are derived from experiments using planar electrodes in traditional H-cells, in which operation is limited to low current densities due to the low concentration of CO_2 in the fully aqueous environment. Whether the nanocubes still display

Received: October 4, 2021
Accepted: January 19, 2022
Published: February 1, 2022

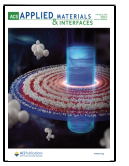

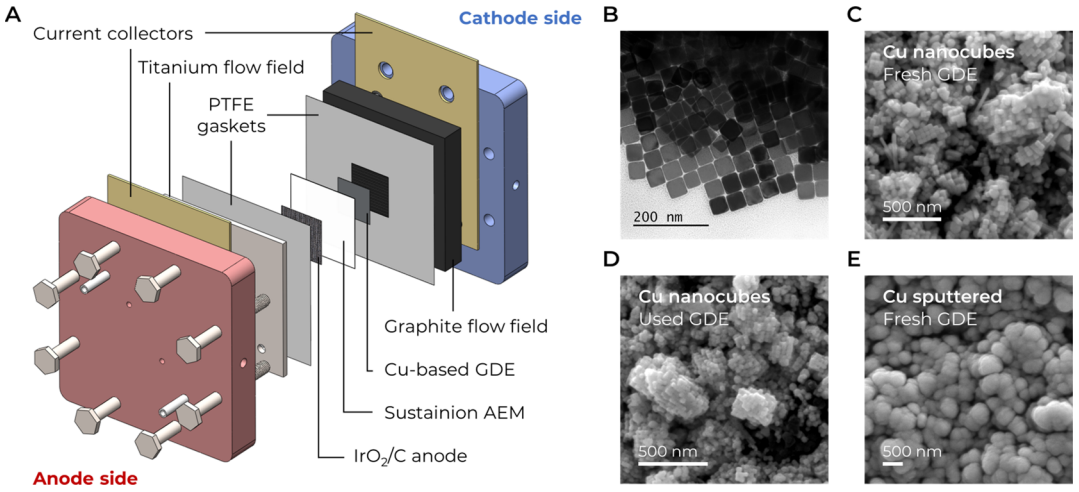

Figure 1. (A) MEA-type electrolytic cell (i.e., with catalyst layers directly in contact with the anion-exchange membrane) with a gas-fed cathode (CO_2, 40 mL_n min^{-1}) and a liquid-fed anode (0.1 M $KHCO_3$). (B) TEM images of the as-synthesized Cu nanocubes. SEM images of the surface of (C) pre- and (D) post-reaction Cu nanocube GDE (Cu_{Cubes}) and of the (E) pre-reaction sputtered Cu GDE.

these desirable catalytic properties when integrated into gas diffusion electrodes (GDEs) which are needed to reach industrially relevant reaction rates (i.e., hundreds of mA cm^{-2}) is still a matter of investigation. A recent study by De Gregorio et al.[16] compared the eCO_2RR performance of GDE-supported copper spheres, octahedra, and nanocubes in a gas-fed electrolyzer with 1 M KOH as the flowing catholyte. While the nanocubes did indeed show high Faradaic efficiencies toward ethylene in this configuration, the presence of a catholyte is problematic from a practical standpoint: on the one hand, CO_2 can be neutralized by the highly alkaline electrolyte even in the absence of current,[17,18] and on the other hand, the presence of a liquid electrolyte between the electrodes causes large ohmic losses.[19] By greatly reducing the interelectrode distance and eliminating the need of a liquid electrolyte between electrodes, zero-gap designs with membrane electrode assemblies (MEAs) can be significantly more energy-efficient.[20,21] However, the reaction environment at the interface between the membrane and the catalyst in a zero-gap cell (e.g., local pH and presence of cations) can be significantly different to that in which a liquid electrolyte is present. In turn, this is expected to influence the catalytic performance and stability of nanostructured catalysts. In this context, we present an investigation of the performance of (100)-oriented copper nanocubes in an MEA-type electrolyzer by comparing them with benchmark electrodes prepared by sputtering, which do not show a preferential orientation. As the first step, the performance of these two catalysts was evaluated at similar mass loadings over a wide range of current densities (20−300 mA cm^{-2}). Following that, we aimed to optimize the mass loading of the nanocube-loaded GDE in order to maximize selectivity toward multicarbon gas products while suppressing the hydrogen evolution reaction (HER).

2. EXPERIMENTAL SECTION

2.1. Cu Nanocube Synthesis and Characterization. Cu nanocubes were synthesized according to a colloidal approach previously reported.[13,15] In a typical synthesis, 9.4 g of tri-*n*-octylphosphine oxide (99%) is added to 117 mL of oleylamine (70%) in a three-necked 250 mL flask connected to a Schlenk line and equipped with a reflux condenser and an internal thermocouple temperature controller. After degassing under vacuum while stirring, 0.71 g of CuBr (99.999%) is added to the solution under nitrogen flow. Then, the mixture is heated to 80 °C and maintained for 15 min, followed by a further increase in temperature to 260 °C. After 1 h at 260 °C, the solution is cooled down to room temperature. With a syringe, the reaction mixture is transferred to vials and then in a glovebox under a protective nitrogen atmosphere, where it is divided in six centrifuge tubes. About 22.5 mL of hexane (96%, anhydrous) is added to each tube (1:1 ratio of solution and hexane) and then centrifuged for 10 min at 6000 rpm. The supernatant is disposed, while the precipitate is recovered in a minimal amount of hexane. To further wash the nanoparticles, an equal amount of ethanol (99.5%, anhydrous) is added, and the resulting solution is centrifuged for another 10 min at 6000 rpm. Finally, the precipitate is recovered with toluene (99.8%, anhydrous) and stored as a solution in a fridge of the glovebox to prevent solvent evaporation before use. Hexane was obtained from Tokyo Chemical Industry, and all other chemicals were obtained from Sigma Aldrich. All the chemicals were used as received, without further purification.

Transmission electron microscopy (TEM) images of Cu nanocubes were acquired on an FEI Tecnai-Spirit at 120 kV. Copper TEM grid (Ted Pella, Inc.) was prepared by drop-casting 10 μL of the nanocube solution.

The concentration of the Cu nanocube solution was determined by inductively coupled plasma optical emission spectrometry (ICP-OES) performed on an Agilent 5100 instrument. The sample aliquot (10 μL) was digested overnight in 285 μL of 70% ICP-grade HNO_3 followed by dilution with deionized water to obtain a 2% acid content needed for the analysis.

2.2. Electrode Preparation. GDEs were prepared by spray-coating Cu nanocube solution on the microporous layer of a Sigracet 39BC gas diffusion layer (GDL, SGL Carbon) with a squared area of 2.25 cm^2. Prior to spray-coating, a concentrated solution of Cu nanocubes in toluene was centrifuged for 10 min at 6000 rpm. The transparent supernatant was disposed and replaced with hexane to obtain 1.5 mL of solution. The solution was sonicated and then loaded in the airbrush reservoir. No ionomer was added because Nafion, the most common one, is insoluble in hexane, which is the solvent where the Cu nanocubes form stable colloidal solutions. The mass of Cu nanocube in the solution was threefold higher than the amount targeted on the electrode. This is necessary because only 33−35% of the active content is actually deposited on the substrate when spraying.[15] This mass loss is partly inherent to the technique (i.e., some of the particles adhere on the walls of the airbrush tank and of the nozzle) and partly due to the use of a mask during spray-coating. An airbrush gun (Fengda BD-138) with a 0.8 mm nozzle was used and the GDL was positioned vertically at 2 cm from the nozzle (Figure S1A). A mask was posed on the GDL during spraying (Figure S1B). While it contributes to mass loss as part of the catalyst deposits

https://doi.org/10.1021/acsami.1c18856
ACS Appl. Mater. Interfaces 2022, 14, 7779−7787

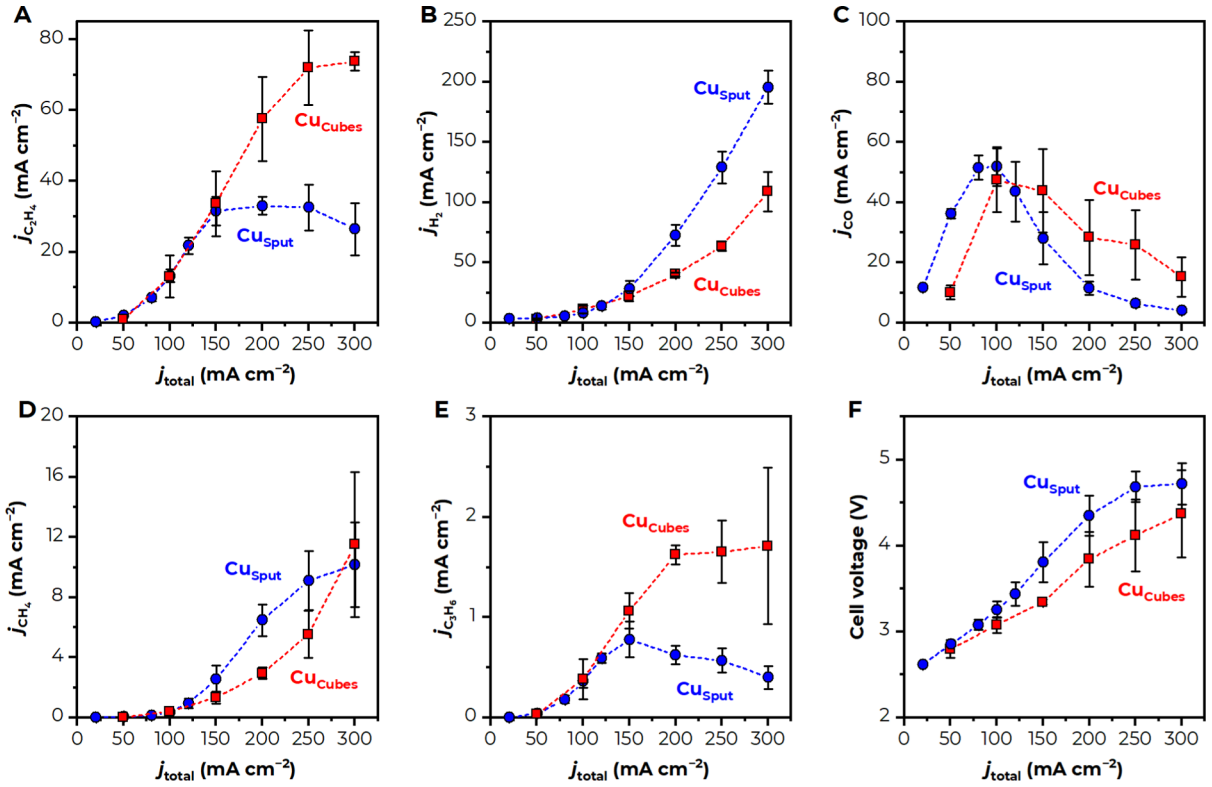

Figure 2. (A–E) Partial current densities (j_i) toward gaseous eCO$_2$RR products as a function of the total current density (j_{total}) over GDEs loaded with Cu nanocubes (Cu$_{Cubes}$, mass loading 440 μg cm^{-2}) and sputtered Cu (Cu$_{Sput}$, mass loading 520 μg cm^{-2}) and (F) corresponding cell voltages, in an MEA-type cell. Current densities and cell voltages are shown as absolute values. Error bars represent the standard error of the mean of three independent measurements. Error bars smaller than the symbol size are omitted for clarity.

on it, the mask avoids edge effects and allows us to obtain a uniform catalyst layer. Spraying (4 s) and pause (4 s) steps were alternated to allow the hexane solvent to evaporate in between deposition as this practice also benefited the homogeneity of the catalyst layer. Scanning electron microscopy (SEM) imaging along with EDX analysis of the Cu-loaded GDL cross section previously demonstrated the homogeneous distribution of the Cu nanocubes within the electrode.[15] Similar data were obtained for the electrodes prepared for this work (Figure S2).

The benchmark electrodes were prepared by direct current magnetron sputtering of a 300 nm film of copper (AJA, purity 99.999%) on carbon paper substrates (Sigracet 39BC) at a power of 115 W in an AJA ATC Orion sputtering system (base pressure < 10^{-7} mTorr). The nominal thickness of the deposited layer was monitored with a quartz crystal microbalance to achieve a catalyst loading of ca. 520 μg cm^{-1}. All cathodes were cut to squares with a geometric area of 2.25 cm^2 for the electrochemical tests.

SEM imaging of the GDEs was carried out in an FEI Quanta 200 FEG instrument operating in the secondary electron mode at an accelerating voltage of 15 kV.

2.3. Cell Configuration and Electrochemical Tests. This work was conducted using a custom-made zero-gap electrolyzer (Figure 1A) equipped with graphite and titanium serpentine flow fields for the cathode and anode, respectively, as described in a previous work,[22] and a BioLogic VSP electrochemical workstation. The cell allows the installation of a reference electrode (leak-free Ag/AgCl, LF-1.6, Innovative Instruments) through a hole of the anodic flow field. Because the tip of the reference electrode has a conductive pathway to the gas-fed cathode, it is possible to carry out simple potentiostatic and potentiodynamic experiments with a gas-fed working electrode in a zero-gap configuration, such as cyclic voltammograms at different scan rates to determine its double layer (DL) capacitance. However, while sufficient for the purposes of the current study, we remark that this electrode placement struggles to accurately determine the cathodic and anodic overpotentials at elevated current densities.[19,23] Commercially available IrO_2-coated carbon paper electrodes (Dioxide Materials, 4.4 cm^2 area), previously described by Kutz et al.,[24] were employed as anodes. A fresh MEA was constructed for each experiment by intercalating a fresh Sustainion X37-50-grade RT anion-exchange membrane (Dioxide Materials, 16 cm^2 area) between the electrodes and fastening the bolts of the cell with a torque of 4 N m. Each electrode was surrounded by poly(tetrafluoroethylene) gaskets (100 μm thickness for the cathode and 250 μm thickness for the anode) to ensure electrical insulation and adequate compression of the MEA components. The cathodic flow field was fed with CO_2 (Air Liquide, purity 4.5 N) at a flow rate of 40 mL$_n$ min^{-1}, which was humidified upstream of the cell by sparging into a container filled with ultrapure water. The sparging vessel was ca. 25 cm high, and on occasion, a slight condensation was soon on the outlet tube, evidencing that the CO_2 was near 100% relative humidity. However, a relative humidity sensor was not used to monitor the outlet gas, so the exact value for a given experiment is not known. Reference conditions for the gas flows in this work are defined as 273.15 K and 1 bar (1 mL$_n$ min^{-1} = 7.434 × 10^{-7} mol s^{-1}). The anodic flow field was fed with a freshly prepared 0.1 M $KHCO_3$ solution (Sigma-Aldrich, 99.995% trace metal basis), which was recirculated continuously at a flow rate of 60 cm^3 min^{-1} using a diaphragm pump. The cathode gas was flowed via a single-pass approach. All tests were carried out at room temperature (ca. 21 °C). While we were consistent in reproducing all of our operating parameters, we did not try to match them identically to any other paper since standard test protocols are yet to be defined in the context of the eCO$_2$RR. Therefore, internal comparisons will be more precise than comparisons to external literature.

2.4. Flow Measurement and Product Analysis. The molar flow rate of the cathodic effluent from the cell was measured continuously with a volumetric flow meter (BPC Instruments AB, μFlow) and all calculations of Faradaic efficiencies and partial current

https://doi.org/10.1021/acsami.1c18856
ACS Appl. Mater. Interfaces 2022, 14, 7779–7787

densities relied on the measured outlet flows to avoid errors.[18] The composition of the gas streams was determined with a PerkinElmer Clarus 580 instrument equipped with Molecular Sieve 13X and HayeSep Q packed columns, operating with argon as a carrier gas at a flow rate of 10 mL min^{-1}. H_2, CO_2, and O_2 were quantified with the thermal conductivity detector, while CO was passed through a methanizer and quantified with the flame ionization detector. GC runs had a duration of 30 min. The long run time allows C3 components to elute from the columns, enabling their detection and quantification.

3. RESULTS AND DISCUSSION

3.1. Catalyst and Electrode Characterization. A representative TEM image of the synthesized Cu nanocubes is shown in Figure 1B. The sample possesses a well-defined cubic morphology with less than 10% being other shapes (i.e., nanorods, bipyramids, and triangles) and a size of 43 ± 4 nm (Figure S3). Figure 1C,D shows the SEM images of a typical GDE prepared from the Cu nanocubes before and after electrolysis, respectively. Further characterization of the same catalysts has been extensively reported in previous work.[14,16,25,26] These data evidence a clear difference in morphology compared to the benchmark electrode prepared with magnetron sputtering. The latter consists of spheroidal Cu particles which expose randomly oriented Cu surfaces (Figure 1E).

3.2. Production Rates of eCO_2RR Gaseous Products over Cu GDEs. Figure 2 shows the partial current densities and the overall cell voltages of the Cu nanocube GDEs and the sputtered Cu benchmark electrodes in an MEA-type cell (i.e., the cathode and anode are directly in contact with the membrane), with humidified CO_2 as the reactant and 0.1 M $KHCO_3$ as the anolyte. The decision to initially use a mass loading of 440 μg cm^{-2} was based on previous optimizations carried out with Cu nanocube-based electrodes.[16] The experiments were carried out in the galvanostatic mode by stepping (at 30 min intervals) the total current density from 20 to 300 mA cm^{-2}. The results reveal the existence of two regions: below 150 mA cm^{-2}, there is little difference in terms of performance between the Cu nanocubes and the benchmark sputtered GDEs, and hydrogen evolution represents only a minor fraction of the total current. On the other hand, above 150 mA cm^{-2}, the two types of electrodes show distinct performance, with a continuous increase in the partial current density for ethylene in the case of the copper nanocubes, whereas ethylene production over the sputtered Cu benchmark begins to decrease and is substituted with the HER. Overall, the results indicate that the Cu nanocube GDEs are capable of achieving considerably higher partial current densities for ethylene (e.g., a twofold higher rate at a total current density of 300 mA cm^{-2}) compared to sputtered copper GDEs, in agreement with previous findings obtained with this type of catalyst in flowing electrolyte cells.[16] In addition, the Cu_{cubes} GDEs showed a significant suppression of hydrogen production and slightly lower production of methane, particularly at elevated total current densities (>150 mA cm^{-2}), as well as lower cell voltages in the surveyed range of current densities with similar mass loadings. Post-reaction SEM images of the Cu nanocube GDE demonstrate that the characteristic morphology of the catalyst was maintained after exposure to reaction conditions (Figure 1D). Overall, these results indicate that the facet-dependent selectivity of the copper nanocubes is conserved in an MEA-type cell at elevated current densities. However, Faradaic efficiencies for the HER tend to be higher in the MEA-type cell, compared to works on a flowing electrolyte configuration. While the reason for this observation is unclear, it is likely a consequence of the intrinsic differences (e.g., pH, presence of cations, reactant accessibility, and flooding characteristics) between the reaction environments at the electrode−membrane interface in an MEA and at the electrode−catholyte interface in a flow cell. Nevertheless, the total cell voltages obtained in the zero-gap cell compare favorably to those in a flowing electrolyte cell due to the minimization of ohmic losses,[16,17] resulting in more energy efficient operation.

Furthermore, we detected the production of propylene at a significant partial current density, particularly over the Cu_{cubes} GDEs (max. $j_{C_3H_6}$ ca. 2 mA cm^{-2}, Figure 2E). While oxygenated compounds (e.g., *n*-propanol and propanaldehyde) are commonly reported C3 products from CO_2 and CO reduction,[27,28] to the best of our knowledge, there is only a single report evidencing the production of the C3 olefin and in such small amounts as to require detection by selected-ion flow tube mass spectrometry.[29] The direct production of propylene by CO_2 reduction is noteworthy both from an applied and fundamental perspective. First, propylene is a major building block in the petrochemical industry (its current spot market price in the United States is ca. 2000 USD per metric ton)[30] and its production via the eCO_2RR might improve the economic perspectives of CO_2 electrolyzers. On the other hand, it might prove challenging to valorize a side product generated in such low rates compared to the target compound (e.g., at 150 mA cm^{-2}, the production rates over Cu nanocubes correspond to only 42 kg of C_3H_6 per metric ton of C_2H_4). Another key issue shown in Figure 3 is that the production of propylene relative to ethylene is actually too high to meet the stringent purity requirements of polymer-grade ethylene (i.e., max. 10−15 ppmv C_3H_6).[31] Therefore, following the removal of excess CO_2 and of the lighter gas products (i.e., H_2, CO, and CH_4) from the electrolyzer effluent, an additional separation step will still be needed at the end of the gas purification train to remove propylene from the final ethylene product. Because this must be considered at the process design level, it would likely have an impact on the technoeconomics of ethylene production via the eCO_2RR.[12,32]

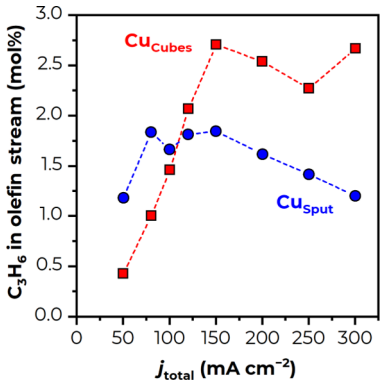

Figure 3. Propylene content in the olefin stream (i.e., only C_2H_4 plus C_3H_6) produced at different total current densities (j_{total}) in an MEA-type cell over GDEs loaded with Cu nanocubes (Cu_{Cubes}) and sputtered Cu (Cu_{Sput}). Because the maximum acceptable concentration of propylene in polymer-grade ethylene is several orders of magnitude lower (i.e., 10−15 ppmv), the production of this commodity chemical via the eCO_2RR would thus require an additional purification step to remove traces of the C3 olefin.

https://doi.org/10.1021/acsami.1c18856
ACS Appl. Mater. Interfaces 2022, 14, 7779−7787

It is important to note, however, that propylene production is not a unique feature of the Cu nanocubes. In fact, the partial current densities of propylene and ethylene appear to be (with a large degree of scatter) linearly correlated both over Cu nanocubes and sputtered Cu, although the values of the former tend to be, in broad terms, around 35 times lower than the latter (Figure S5). This helps explain the scarcity of reports of propylene production: GC methods used in CO_2 reduction are typically optimized for speed, concluding the analysis after the elution of C2 compounds and, particularly when using traditional H-cells with planar electrodes, the concentration of generated propylene would typically fall below the limit of detection.

Recent studies have shown that the loss of eCO_2RR activity (and the switch of selectivity toward the HER) at high current densities over carbon-based GDEs is the result of the loss of hydrophobicity and subsequent flooding, although the mechanism behind this is still a matter of discussion.[16,33−35] To investigate whether flooding was affecting the performance of our GDEs, we monitored the DL capacitance of the electrodes after each galvanostatic step. The DL capacitance serves as a proxy variable for the wetted electrode area, thus providing an indication of the extent of flooding.[33] Both the Cu_{Cubes} and Cu_{Sput} electrodes have an initial DL capacitance that is an order of magnitude higher than that of the bare GDL, showing that both forms of the catalyst provide a high electrochemically active surface area (ECSA). Nevertheless, the initial DL capacitance of the Cu nanocube GDE is slightly lower, which is likely a reflection of the slightly lower mass loading of the electrode compared to the sputtered Cu sample. Figure 4 shows that, in both electrodes, there is a sharp

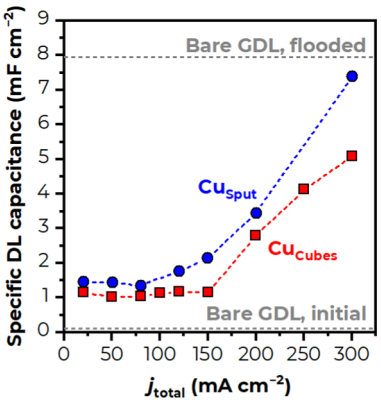

Figure 4. Specific DL capacitance of GDEs loaded with Cu nanocubes (Cu_{Cubes}) and sputtered Cu (Cu_{Sput}) at different total current densities (j_{total}) in an MEA-type cell. The dashed horizontal lines indicate the capacitance of the fresh and flooded bare GDL.

increase in the DL capacitance at current densities above 120−150 mA cm^{-2}, evidencing the onset of electrode flooding. However, unlike the benchmark electrode, the Cu_{Cubes} GDE is capable of sustaining a high rate of ethylene production even when it is flooded. This is likely a result of the different distribution of the catalyst between these two GDEs. In the case of the Cu_{Sput} electrode, the catalyst is concentrated in a very limited region which, due to its proximity to the membrane, is (a) likely quicker to flood thoroughly and (b) imposes a more tortuous path for the CO_2 reactant, worsening mass transfer limitations. In contrast, the homogeneous distribution of the Cu_{Cubes} GDE probably leads to a situation in which at least part of the catalyst is still accessible to CO_2 despite some sections of the electrode being flooded already.

It should be noted that the incoming cathodic gas was near 100% relative humidity. Given that humidity is known to affect performance, potentially operating at lower humidity could have extended the time before flooding was evidenced. However, analyzing the impact of humidity bring an extra layer of complexity to the analysis and is beyond the scope of this work but is a logical next parameter to investigate.[36−38] In addition, increasing reactor temperature could also help to keep a drier cathode for longer,[39] but if there is a corrosion mechanism with the hydrophobic units of the GDL, this could also speed that up. Increasing temperature will decrease CO_2 solubility and likely affect product selectivity. Therefore, temperature is also a very interesting but potentially complex variable to analyze, which will be undertaken in future work.

Considering the capacity shown by the Cu_{Cubes} GDE to operate at elevated current densities and maintain a high FE toward ethylene despite the onset of flooding, we evaluated its stability at a constant current density of 250 mA cm^{-2} (Figure 5). After an induction period, the Faradaic efficiency toward

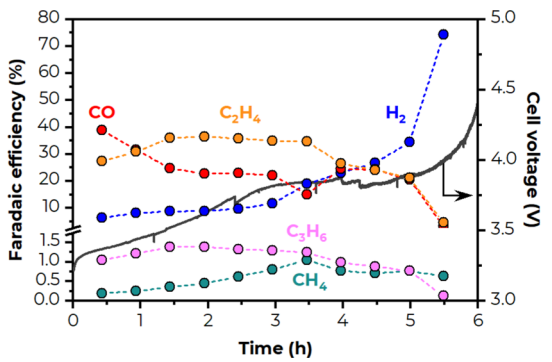

Figure 5. Faradaic efficiency for eCO_2RR gas products and cell voltage during a stability test of a Cu_{Cubes} GDE (loading 440 μg cm^{-2}) operating at a constant current density of 250 mA cm^{-2}.

ethylene plateaus at ca. 35% and the selectivity toward hydrogen evolution is relatively low (i.e., below 10%). However, the performance of the electrode degraded rapidly after the 3 h mark, potentially as a result of cumulative flooding that cannot be counteracted anymore by the homogeneous distribution of the nanocubes within the GDL. While the stability of the Cu nanocubes at high current densities in a zero-gap configuration compares favorably to similar studies in a flow cell (i.e., with a liquid catholyte),[16] these results echo recent reports in the literature suggesting that water management of the cathodic GDE is crucial to attain high and stable eCO_2RR performance at elevated current densities.[33,34]

3.3. Influence of Electrode Loading. At a j_{total} below 100 mA cm^{-2}, the Cu nanocube GDE showed relatively high selectivity toward CO but a low figure for C_2H_4 (ca. 60−70% vs 0−5%, respectively, Figure 6), suggesting that, under those operating conditions, the cathodic overpotential is likely still too low to drive C−C coupling. While it would be reasonable to attempt to maximize the rate of production of ethylene by operating the electrolyzer at the highest possible current density, another viable strategy is to operate at lower total current densities—at which, the electrode is less prone to flooding—and focus on trying to shift the selectivity toward C_2H_4 and away from CO by driving the cathode to higher

https://doi.org/10.1021/acsami.1c18856
ACS Appl. Mater. Interfaces 2022, 14, 7779−7787

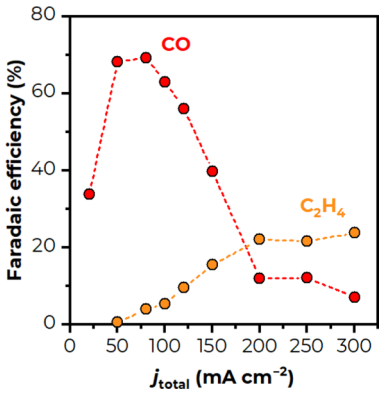

Figure 6. Faradaic efficiencies for CO and C_2H_4 over a Cu_{Cubes} GDE with a high catalyst mass loading (440 μg cm^{-2}), evidencing high selectivity toward CO at low current densities.

overpotentials. To this end, we explored whether decreasing the mass loading of the electrode (in effect, decreasing the ECSA of the catalyst layer) improves the production of C_2H_4 by imposing a requirement for a higher cathodic overpotential at lower total (geometric) current densities. However, we remark that this positive effect might in practice be offset by the occurrence of mass transfer limitations at lower current densities caused by the decreased mass loadings.

Figure 7 shows the electrocatalytic performance of the Cu nanocube GDEs with decreased mass loadings compared to the high-loading benchmark shown previously. It is interesting to note that at low current densities, the cell voltages with the lower-loading electrodes are ca. 200 mV higher (Figure 7F, inset). Even though it was not possible to deconvolute the individual electrode overpotentials in our zero-gap electrolyzer, we remark that because both the anode and membrane are the same (and thus should display a similar overpotential and resistance, respectively, at the same j_{total}), the higher cell voltage is most likely a reflection of a higher cathodic overpotential when the lower-loading GDEs were used. However, we note that the relationship between the increased overpotential and the measured current densities does not conform to a Tafel behavior, suggesting that there must be other effects (e.g., local pH issues and highly active sites becoming mass transfer-limited) behind the difference with the high-loading benchmark. In any case, we found that as intended, the selectivity shifted away from CO and toward ethylene, reaching a maximum of ca. 40% at a j_{total} of 150−200 mA cm^{-2}. This increased selectivity toward ethylene translates into a higher maximum production rate of ethylene (ca. 90 mA cm^{-2}, Figure S6) despite the lower total current density. However, ethylene production at higher current densities (j_{total} > 200 mA cm^{-2}) suffers possibly because mass transfer limitations caused by flooding are exacerbated by the lower catalyst loadings. This effect is particularly noticeable in the lowest-loading electrode (111 μg cm^{-2}), in which eCO_2RR selectivity at high current densities (i.e., under flooded operation) shifted to methane despite showing similar cell voltages. However, it is important to note that electrodes with lower catalyst loadings are in general more sensitive to any contaminations present in the system. Based on these results and taking into account that (a) galvanostatic operation is

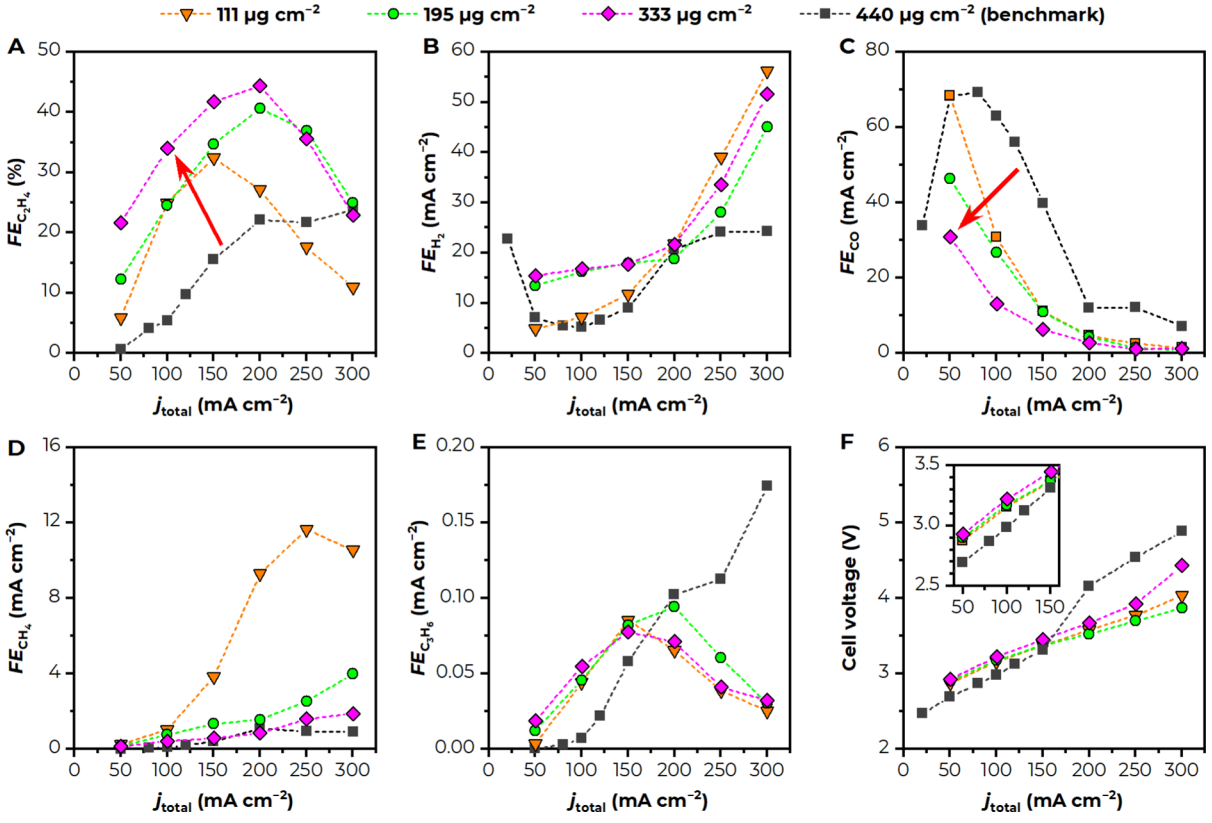

Figure 7. (A−E) Faradaic efficiencies (FE_i) toward gaseous eCO_2RR products as a function of the total current density (j_{total}) over GDEs loaded with Cu nanocubes with different mass loadings and (F) corresponding cell voltages, in an MEA-type cell. Current densities and cell voltages are shown as absolute values. The red arrows indicate the performance shift from the high-loading benchmark sample.

https://doi.org/10.1021/acsami.1c18856
ACS Appl. Mater. Interfaces 2022, 14, 7779−7787

typically preferred in bulk electrosynthetic processes and that (b) the eCO_2RR selectivity of Cu-based catalysts changes drastically with the overpotential, the mass loading of the GDE emerges as a simple but important parameter that needs to be tailored to the intended operating (geometric) current density. Ongoing studies in our group aim to unveil the effect of the mass loading and catalytic ECSA of the GDE on the onset of mass transfer limitations and the developed cathodic overpotential under different conditions under galvanostatic operation.

It should be noted that while adding fillers such as a carbon-based catalyst support would presumably be able to enhance particle dispersion, it also adds a material whose influence in the eCO_2RR is unclear. As mentioned previously, the low loadings are already susceptible toward contamination and adding something such as carbon black or nanotubes could provide an additional source of contamination. Furthermore, it has been reported that carbon does produce a notable amount of hydrogen; this issue could complicate the understanding of the intrinsic behavior of the copper catalyst itself.

4. CONCLUSIONS

In this work, we investigated the performance toward gaseous CO_2 reduction products of GDEs loaded with copper nanocubes in a zero-gap, MEA-type electrolyzer. Compared to benchmark electrodes prepared by sputtering copper on the same carbon-based substrate, Cu nanocube-loaded GDEs achieved higher production rates of ethylene (j_{C2H4} up to ca. 80 mA cm^{-2}) by maintaining high Faradaic efficiencies at elevated current densities (i.e., >150 mA cm^{-2}), demonstrating the preservation of the facet-dependent selectivity of the nanocube morphology. In addition, CO_2 reduction to propylene—a seldom reported product with intrinsic industrial value—was observed over both nanocube and sputtered Cu catalysts, with the former showing slightly higher selectivities and production rates due to its higher overall propensity toward multicarbon products. DL capacitance measurements of both types of electrodes indicated the onset of flooding above a current density of 150 mA cm^{-2}, although Cu nanocube GDEs were able to still maintain high rates of ethylene production under flooded operation and showed stable CO_2 reduction with low HER for ca. 3 h at a total current density of 250 mA cm^{-2}. By decreasing the mass loading of the Cu nanocube GDEs, it was possible to improve the selectivity toward ethylene when operating at lower total current densities (i.e., below 150 mA cm^{-2}), at the expense of performance at higher current densities. Ongoing areas of work include tailoring the mass loading (and catalytic ECSA) to the desired operating conditions and developing strategies to mitigate the flooding-induced loss of ethylene selectivity of Cu nanocube-loaded electrodes.

ASSOCIATED CONTENT

Supporting Information

The Supporting Information is available free of charge at https://pubs.acs.org/doi/10.1021/acsami.1c18856.

Size distribution of the as-synthesized Cu nanocubes derived from TEM imaging; Faradaic efficiencies over GDEs loaded with Cu nanocubes and sputtered Cu; partial current densities for ethylene and propylene over all Cu-loaded GDEs; and partial current densities over GDEs loaded with Cu nanocubes with different mass loadings (PDF)

AUTHOR INFORMATION

Corresponding Author

Brian Seger − *Section for Surface Physics and Catalysis (SurfCat), Department of Physics, Technical University of Denmark, 2800 Kgs. Lyngby, Denmark;* orcid.org/0000-0002-0036-095X; Phone: +45 45 25 33 44; Email: brse@fysik.dtu.dk

Authors

Gastón O. Larrazábal − *Section for Surface Physics and Catalysis (SurfCat), Department of Physics, Technical University of Denmark, 2800 Kgs. Lyngby, Denmark;* Present Address: Green Hydrogen Systems A/S, 6000 Kolding, Denmark; orcid.org/0000-0003-4218-3514

Valery Okatenko − *Laboratory of Nanochemistry for Energy, Institute of Chemical Sciences and Engineering, Ecole Polytechnique Fédérale de Lausanne, 1950 Sion, Switzerland*

Ib Chorkendorff − *Section for Surface Physics and Catalysis (SurfCat), Department of Physics, Technical University of Denmark, 2800 Kgs. Lyngby, Denmark;* orcid.org/0000-0003-2738-0325

Raffaella Buonsanti − *Laboratory of Nanochemistry for Energy, Institute of Chemical Sciences and Engineering, Ecole Polytechnique Fédérale de Lausanne, 1950 Sion, Switzerland;* orcid.org/0000-0002-6592-1869

Complete contact information is available at: https://pubs.acs.org/10.1021/acsami.1c18856

Author Contributions

G.O.L. carried out the electrochemical tests and prepared the sputtered Cu electrodes. V.O. carried out the nanocube catalyst synthesis and prepared the electrodes. G.O.L. performed the data analysis and wrote the manuscript with input from all co-authors. I.C., R.B., and B.S. conceived the project and oversaw its development.

Notes

The authors declare no competing financial interest.

ACKNOWLEDGMENTS

G.O.L. acknowledges funding from the European Union's Horizon 2020 research and innovation program through a Marie Skłodowska-Curie Individual Fellowship under grant agreement 844288 (STRATCAT-CO_2). B.S acknowledges funding from the Villum Foundation V-SUSTAIN grant 9455 to the Villum Center for the Science of Sustainable Fuels and Chemicals and the ECOEthylene project from the Innovation Fund Denmark (Grant# 8057-00018B). V.O. acknowledges funding from the Swiss National Science Foundation, project number 200021L_191997.

REFERENCES

(1) Kondratenko, E. V.; Mul, G.; Baltrusaitis, J.; Larrazábal, G. O.; Pérez-Ramírez, J. Status and Perspectives of CO_2 Conversion into Fuels and Chemicals by Catalytic, Photocatalytic and Electrocatalytic Processes. *Energy Environ. Sci.* **2013**, *6*, 3112−3135.

(2) Chen, A.; Lin, B.-L. A Simple Framework for Quantifying Electrochemical CO_2 Fixation. *Joule* **2018**, *2*, 594−606.

(3) Bushuyev, O. S.; De Luna, P.; Dinh, C. T.; Tao, L.; Saur, G.; van de Lagemaat, J.; Kelley, S. O.; Sargent, E. H. What Should We Make with CO_2 and How Can We Make It? *Joule* **2018**, *2*, 825−832.

(4) Nitopi, S.; Bertheussen, E.; Scott, S. B.; Liu, X.; Engstfeld, A. K.; Horch, S.; Seger, B.; Stephens, I. E. L.; Chan, K.; Hahn, C.; Nørskov, J. K.; Jaramillo, T. F.; Chorkendorff, I. Progress and Perspectives of Electrochemical CO_2 Reduction on Copper in Aqueous Electrolyte. *Chem. Rev.* **2019**, *119*, 7610−7672.
(5) Hori, Y.; Kikuchi, K.; Suzuki, S. Production of CO and CH_4 in Electrochemical Reduction of CO_2 at Metal Electrodes in Aqueous Hydrogencarbonate Solution. *Chem. Lett.* **1985**, *14*, 1695−1698.
(6) Kuhl, K. P.; Cave, E. R.; Abram, D. N.; Jaramillo, T. F. New Insights into the Electrochemical Reduction of Carbon Dioxide on Metallic Copper Surfaces. *Energy Environ. Sci.* **2012**, *5*, 7050.
(7) Clark, E. L.; Bell, A. T. Chapter 3 Heterogeneous Electrochemical CO_2 Reduction. In Carbon Dioxide Electrochemistry: Homogeneous and Heterogeneous Catalysis. *R. Soc. Chem.* **2021**, 98−150.
(8) Hori, Y.; Takahashi, I.; Koga, O.; Hoshi, N. Selective Formation of C2 Compounds from Electrochemical Reduction of CO_2 at a Series of Copper Single Crystal Electrodes. *J. Phys. Chem. B* **2002**, *106*, 15−17.
(9) Schouten, K. J. P.; Qin, Z.; Pérez Gallent, E.; Koper, M. T. M. Pérez Gallent, E.; Koper, M. T. M. Two Pathways for the Formation of Ethylene in CO Reduction on Single-Crystal Copper Electrodes. *J. Am. Chem. Soc.* **2012**, *134*, 9864−9867.
(10) Hahn, C.; Hatsukade, T.; Kim, Y.-G.; Vailionis, A.; Baricuatro, J. H.; Higgins, D. C.; Nitopi, S. A.; Soriaga, M. P.; Jaramillo, T. F. Engineering Cu Surfaces for the Electrocatalytic Conversion of CO_2: Controlling Selectivity toward Oxygenates and Hydrocarbons. *Proc. Natl. Acad. Sci. U.S.A.* **2017**, *114*, 5918.
(11) Liu, X.; Xiao, J.; Peng, H.; Hong, X.; Chan, K.; Nørskov, J. K. Understanding Trends in Electrochemical Carbon Dioxide Reduction Rates. *Nat. Commun.* **2017**, *8*, 15438.
(12) Ioannou, I.; D'Angelo, S. C.; Martín, A. J.; Pérez-Ramírez, J.; Guillén-Gosálbez, G. Hybridization of Fossil- and CO_2-Based Routes for Ethylene Production Using Renewable Energy. *ChemSusChem* **2020**, *13*, 6370−6380.
(13) Roberts, F. S.; Kuhl, K. P.; Nilsson, A. High Selectivity for Ethylene from Carbon Dioxide Reduction over Copper Nanocube Electrocatalysts. *Angew. Chem. Int. Ed.* **2015**, *54*, 5179−5182.
(14) Loiudice, A.; Lobaccaro, P.; Kamali, E. A.; Thao, T.; Huang, B. H.; Ager, J. W.; Buonsanti, R. Tailoring Copper Nanocrystals towards C2 Products in Electrochemical CO_2 Reduction. *Angew. Chem. Int. Ed.* **2016**, *55*, 5789−5792.
(15) Mangione, G.; Huang, J.; Buonsanti, R.; Corminboeuf, C. Dual-Facet Mechanism in Copper Nanocubes for Electrochemical CO_2 Reduction into Ethylene. *J. Phys. Chem. Lett.* **2019**, *10*, 4259−4265.
(16) De Gregorio, G. L.; Burdyny, T.; Loiudice, A.; Iyengar, P.; Smith, W. A.; Buonsanti, R. Facet-Dependent Selectivity of Cu Catalysts in Electrochemical CO_2 Reduction at Commercially Viable Current Densities. *ACS Catal.* **2020**, *10*, 4854−4862.
(17) Ma, M.; Clark, E. L.; Therkildsen, K. T.; Dalsgaard, S.; Chorkendorff, I.; Seger, B. Insights into the Carbon Balance for CO_2 Electroreduction on Cu Using Gas Diffusion Electrode Reactor Designs. *Energy Environ. Sci.* **2020**, *13*, 977−985.
(18) Larrazábal, G. O.; Ma, M.; Seger, B. A Comprehensive Approach to Investigate CO_2 Reduction Electrocatalysts at High Current Densities. *Acc. Mater. Res.* **2021**, *2*, 220−229.
(19) Salvatore, D.; Berlinguette, C. P. Voltage Matters When Reducing CO_2 in an Electrochemical Flow Cell. *ACS Energy Lett.* **2020**, *5*, 215−220.
(20) Higgins, D.; Hahn, C.; Xiang, C.; Jaramillo, T. F.; Weber, A. Z. Gas-Diffusion Electrodes for Carbon Dioxide Reduction: A New Paradigm. *ACS Energy Lett.* **2019**, *4*, 317−324.
(21) Weng, L.-C.; Bell, A. T.; Weber, A. Z. Towards Membrane-Electrode Assembly Systems for CO_2 Reduction: A Modeling Study. *Energy Environ. Sci.* **2019**, *12*, 1950−1968.
(22) Larrazábal, G. O.; Strøm-Hansen, P.; Heli, J. P.; Zeiter, K.; Therkildsen, K. T.; Chorkendorff, I.; Seger, B. Analysis of Mass Flows and Membrane Cross-over in CO_2 Reduction at High Current Densities in an MEA-Type Electrolyzer. *ACS Appl. Mater. Interfaces* **2019**, *11*, 41281−41288.
(23) He, W.; Nguyen, T. V. Edge Effects on Reference Electrode Measurements in PEM Fuel Cells. *J. Electrochem. Soc.* **2004**, *151*, A185.
(24) Kutz, R. B.; Chen, Q.; Yang, H.; Sajjad, S. D.; Liu, Z.; Masel, I. R. Sustainion Imidazolium-Functionalized Polymers for Carbon Dioxide Electrolysis. *Energy Technol.* **2017**, *5*, 929−936.
(25) Huang, J.; Hörmann, N.; Oveisi, E.; Loiudice, A.; De Gregorio, G. L.; Andreussi, O.; Marzari, N.; Buonsanti, R. Potential-Induced Nanoclustering of Metallic Catalysts during Electrochemical CO_2 Reduction. *Nat. Commun.* **2018**, *9*, 3117.
(26) Iyengar, P.; Kolb, M. J.; Pankhurst, J. R.; Calle-Vallejo, F.; Buonsanti, R. Elucidating the Facet-Dependent Selectivity for CO_2 Electroreduction to Ethanol of Cu-Ag Tandem Catalysts. *ACS Catal.* **2021**, *11*, 4456−4463.
(27) Li, J.; Che, F.; Pang, Y.; Zou, C.; Howe, J. Y.; Burdyny, T.; Edwards, J. P.; Wang, Y.; Li, F.; Wang, Z.; De Luna, P.; Dinh, C. T.; Zhuang, T. T.; Saidaminov, M. I.; Cheng, S.; Wu, T.; Finfrock, Y. Z.; Ma, L.; Hsieh, S. H.; Liu, Y. S.; Botton, A. G.; Pong, W. F.; Du, X.; Guo, J.; Sham, T. K.; Sargent, E. H.; Sinton, D.; et al. Copper Adparticle Enabled Selective Electrosynthesis of N-Propanol. *Nat. Commun.* **2018**, *9*, 4614.
(28) Bertheussen, E.; Hogg, T. V.; Abghoui, Y.; Engstfeld, A. K.; Chorkendorff, I.; Stephens, I. E. L. Electroreduction of CO on Polycrystalline Copper at Low Overpotentials. *ACS Energy Lett.* **2018**, *3*, 634−640.
(29) Mandal, L.; Yang, K. R.; Motapothula, M. R.; Ren, D.; Lobaccaro, P.; Patra, A.; Sherburne, M.; Batista, V. S.; Yeo, B. S.; Ager, J. W.; Martin, J.; Venkatesan, T. Investigating the Role of Copper Oxide in Electrochemical CO_2 Reduction in Real Time. *ACS Appl. Mater. Interfaces* **2018**, *10*, 8574−8584.
(30) Torres, A.; Hays, K. US spot polymer-grade propylene prices spike to a near-decade high. https://www.spglobal.com/platts/en/market-insights/latest-news/petrochemicals/020521-featureus-spot-polymer-grade-propylene-prices-spike-to-a-near-decade-high. (accessed Feb 5, 2021).
(31) Immermann, H. E. Z.; Division, L. E. Ethylene. *Ullmann's Encyclopedia of Industrial Chemistry*, Wiley-VCH; 2010.
(32) Jouny, M.; Luc, W.; Jiao, F. General Techno-Economic Analysis of CO_2 Electrolysis Systems. *Ind. Eng. Chem. Res.* **2018**, *57*, 2165−2177.
(33) Leonard, M. E.; Clarke, L. E.; Forner-Cuenca, A.; Brown, S. M.; Brushett, F. R. Investigating Electrode Flooding in a Flowing Electrolyte, Gas-Fed Carbon Dioxide Electrolyzer. *ChemSusChem* **2020**, *13*, 400−411.
(34) Yang, K.; Kas, R.; Smith, W. A.; Burdyny, T. Role of the Carbon-Based Gas Diffusion Layer on Flooding in a Gas Diffusion Electrode Cell for Electrochemical CO_2 Reduction. *ACS Energy Lett.* **2021**, *6*, 33−40.
(35) Leonard, M. E.; Orella, M. J.; Aiello, N.; Román-Leshkov, Y.; Forner-Cuenca, A.; Brushett, F. R. Editors' Choice-Flooded by Success: On the Role of Electrode Wettability in CO_2 Electrolyzers that Generate Liquid Products. *J. Electrochem. Soc.* **2020**, *167*, 124521.
(36) Lee, W.; Kim, Y. E.; Youn, M. H.; Jeong, S. K.; Park, K. T. Catholyte-Free Electrocatalytic CO_2 Reduction to Formate. *Angew. Chem., Int. Ed.* **2018**, *57*, 6883−6887.
(37) Díaz-Sainz, G.; Alvarez-Guerra, M.; Solla-Gullón, J.; García-Cruz, L.; Montiel, V.; Irabien, A. Gas−Liquid−Solid Reaction System for CO_2 Electroreduction to Formate without Using Supporting Electrolyte. *AIChE J.* **2020**, *66*, No. e16299.
(38) De Mot, B.; Ramdin, M.; Hereijgers, J.; Vlugt, T. J. H.; Breugelmans, T. Direct Water Injection in Catholyte-Free Zero-Gap Carbon Dioxide Electrolyzers. *ChemElectroChem* **2020**, *7*, 3839−3843.
(39) Díaz-Sainz, G.; Alvarez-Guerra, M.; Ávila-Bolívar, B.; Solla-Gullón, J.; Montiel, V.; Irabien, A. Improving Trade-Offs in the Figures of Merit of Gas-Phase Single-Pass Continuous CO_2

https://doi.org/10.1021/acsami.1c18856
ACS Appl. Mater. Interfaces 2022, 14, 7779−7787

Electrocatalytic Reduction to Formate. *Chem. Eng. J.* **2021**, *405*, 126965.

https://doi.org/10.1021/acsami.1c18856
ACS Appl. Mater. Interfaces 2022, 14, 7779−7787